Earth and Planetary Science Letters 548 (2020) 116490

Contents lists available at ScienceDirect

Earth and Planetary Science Letters

www.elsevier.com/locate/epsl

Record of intermediate-depth subduction seismicity in a dry slab from an exhumed ophiolite

G. Pennacchioni [a,*], M. Scambelluri [b], M. Bestmann [c], L. Notini [b], P. Nimis [a], O. Plümper [d], M. Faccenda [a], F. Nestola [a]

[a] Dipartimento di Geoscienze, Università di Padova, Via G. Gradenigo 6, 35131 Padova, Italy
[b] Dipartimento di Scienze della Terra, Ambiente e Vita, University of Genova, Corso Europa 26, 16132 Genova, Italy
[c] GeoZentrum Nordbayern, Friedrich-Alexander-Universität Erlangen-Nürnberg (FAU), Germany
[d] Department of Earth Sciences, Utrecht University, the Netherlands

ARTICLE INFO

Article history:
Received 22 April 2020
Received in revised form 25 June 2020
Accepted 16 July 2020
Available online 12 August 2020
Editor: A. Yin

Keywords:
ophiolite
earthquake
subduction
pseudotachylyte
eclogite
fluids

ABSTRACT

The ophiolitic peridotite and gabbro of Moncuni (Southern Lanzo Massif, Western Alps) retain pre-subduction mantle-to-oceanic, high-temperature (> 700 °C) ductile fabrics. These fabrics are overprinted by seismic fracturing and faulting associated with pseudotachylytes. Within the gabbro, the pseudotachylytes preserve dry glass and pristine microlites. The occurrence of rare, minute garnet and the static development of eclogite-facies assemblages in local hydrated domains indicate that pseudotachylytes experienced subduction conditions of 600 °C and 2.1 GPa. The exceptional survival of glass and the absence of post-oceanic ductile deformation demonstrate prevailing dry conditions during the entire Alpine subduction and exhumation path. Dry conditions inhibited reaction kinetics and viscous flow. In contrast, the majority of the Alpine ophiolites, derived from the upper hydrated portions of the oceanic lithosphere, show pervasive fluid-assisted metamorphism and ductile deformation. The Moncuni body can, therefore, be regarded as representative for the rheological behaviour during subduction of seismic, dry, deeper oceanic lithosphere that is rarely exhumed to the Earth's surface. In Moncuni, the brittle-ductile transition of dry oceanic rocks is constrained to be between 600 and 750 °C. This temperature range corresponds to the observed cut-off of intermediate-depth seismicity within subducting slabs. We infer that the base of the seismic layer corresponds to the brittle-ductile transition of a dry slab rather than the locus of antigorite breakdown triggering earthquakes by dehydration embrittlement.

1. Introduction

Subduction is a key global process that has been affecting Earth's evolution by shaping the continents and driving the formation of new continental crust and major volcanic fronts. Stress build-up at convergent plate boundaries continuously induces seismic activity that has a big societal impact. However, the subduction processes are inaccessible to direct investigation: our understanding of their chemical-physical mechanisms relies on geophysical data, laboratory experiments and numerical modelling. Complementary information is provided by the studies of rocks that are tectonically exhumed from depth to the Earth's surface and represent the geological record of deep-seated geologic processes.

An enormous geophysical dataset forms the basis for earthquake nucleation models and associated deformation processes. For intermediate-depth (50–300 km) subduction earthquakes, the geophysical data shows the occurrence of double seismic zones in most subducting slabs. These zones consist of one seismic layer immediately below the interface between converging plates (upper plane of seismicity: UPS) and a second one 15–30 km inside the mantle of the subducting lithospheric plate (lower plane of seismicity: LPS) (Hacker et al., 2003; Yamasaki and Seno, 2003; Brudzinski et al., 2007). The origin of double seismic zones and of intermediate-depth subduction seismicity remains debated. A central question is whether LPS earthquakes occur within a dry mantle (e.g. Reynard et al., 2010) or a hydrated (serpentinized) mantle (Seno and Yamanaka, 1996; Peacock, 2001; Yamasaki and Seno, 2003). The same question applies to the basal part of the UPS (Scambelluri et al., 2017). Several authors have proposed that earthquake nucleation in subduction zones is the result of fluid pressure build-up during the breakdown of hydrous minerals (e.g. Kirby et al., 1996; Jung et al., 2004; Dobson et al., 2002), a mechanism typically referred to as dehydration embrittlement. Another suggested mechanism for the development of intermediate-depth

* Corresponding author.
E-mail address: giorgio.pennacchioni@unipd.it (G. Pennacchioni).

https://doi.org/10.1016/j.epsl.2020.116490
0012-821X/

subduction earthquakes is self-localizing thermal runaway (Kelemen and Hirth, 2007; John et al., 2009).

Although the nucleation mechanism for intermediate-depth earthquakes remains unknown, the geological record of intermediate-depth earthquakes is potentially stored in ophiolites (remnants of oceanic lithosphere incorporated in collisional belts) that experienced subduction. Subduction of ophiolites is recorded by blueschist- to eclogite-facies metamorphic assemblages. However, evidence of the extensive seismicity of subduction zones remains elusive in high-pressure ophiolites for several reasons. First, exhumed ophiolites are not representative of the whole seismic structure of subducting oceanic slabs, as the slivers of oceanic lithosphere incorporated within accretionary wedges and collisional belts almost entirely belong to the uppermost, hydrated top of the oceanic lithospheric slab. Second, pseudotachylytes (fault rocks formed by quenching of frictional melts, widely considered diagnostic of coseismic slip: Sibson, 1975), developed under blueschist-eclogite-facies conditions, have been reported so far for only two localities (Corsica: Andersen and Austrheim, 2006; Fabbri et al., 2018; Moncuni, Lanzo: Scambelluri et al., 2017). These pseudotachylytes are found in peridotite-gabbro massifs preserving ample portions of pristine, dry rocks. In contrast, the much more common hydrated ophiolites preserve relatively frequent synkinematic high-pressure veins and/or breccias that could be consistent with the process of dehydration embrittlement. The seismic origin of these eclogite-facies veins and breccias (Locatelli et al., 2018), although possible, is difficult to verify.

Here we investigate the ophiolitic peridotite and gabbro from the Moncuni area (Lanzo Ultramafic Massif, Western Alps). During the Alpine orogeny, these rocks were subducted to eclogite-facies conditions and then exhumed without experiencing ductile deformation and metamorphism. We show that the Moncuni rocks remained dry throughout their geological history and behaved in a brittle fashion during the whole subduction-exhumation cycle. Pervasive seismic faulting is recorded by the occurrence of pseudotachylytes (Piccardo et al., 2007, 2010; Scambelluri et al., 2017) and by diffuse cataclastic deformation associated with intense *in-situ* "pulverization" (Petley-Ragan et al., 2019; Incel et al., 2019). We suggest that the deformation behaviour observed in these exhumed rocks can be a proxy for the rheology of the seismogenic part of the oceanic slab at intermediate-depth.

2. Methods

Backscattered electron (BSE, atomic Z-contrast) imaging was performed on SYTON-polished, carbon-coated (coating thickness: 4 nm) thin sections, using a ZEISS Cross-Beam 1540 EsB SEM equipped with a thermo-ionic field emission gun at the Department Werkstoffwissenschaften – FAU Erlangen-Nürnberg University. Working conditions were: 9 mm working distance, 20 kV acceleration voltage, 120 mm aperture and ~ 7 nA beam current.

Electron backscatter diffraction (EBSD) maps were acquired at 20 kV and 9.54 nA, with a step size of 0.7 µm, using a Philips XL30 ESEM FEG equipped with an Oxford Instruments Nordlys 2 CCD camera and Oxford Instrument software AZtec at Utrecht University. Raw crystal orientation maps were processed, after noise reduction filtering and elimination of systematic misindexing, using the Oxford Instrument software Channel5. A misorientation of 10° was used to distinguish subgrains from new grains.

Microchemical analyses were performed with a CAMECA SX-50 electron microprobe (IGG–CNR, Padua, Italy) equipped with four wavelength-dispersive spectrometers. Natural and synthetic standards (diopside for Mg, Ca and Si, albite for Na, orthoclase for K, and pure Al, Cr, Fe, and Mn–Ti oxides) were used. For olivine, Mg was calibrated on natural forsterite. Analytical conditions were: (i) 15 kV accelerating voltage, 20 nA beam current, and 1 µm beam size (for mineral analysis); and (ii) 20 kV accelerating voltage, 2 nA (Na, K, Al, Si) to 20 nA (all other elements) beam current (for pseudotachylyte glass). Acquisition times were: 10 s and 5 s for both peak and background measurements, respectively. For Na, K, Al, Si analysis of glass, counting times of 10 s were used for background measurements.

Micro-Raman measurements were conducted in backscattering geometry with a Horiba Jobin-Yvon Explora_Plus spectrometer equipped with an Olympus BX41 microscope holding a long-working distance objective with a 100× magnification and ~ 1 µm spatial resolution. The spectrometer is at the Department of Earth, Environment and Life Sciences, University of Genova. The spectrometer was calibrated to the silicon Raman peak at 520.5 cm^{-1}. The spectral resolution was ~ 2 cm^{-1} and the instrumental accuracy at peak position was 0.5 cm^{-1}. The measurements were done with two different lasers in order to avoid luminescence effects. Raman spectra at low wavenumber range (between 100 cm^{-1} and 1300 cm^{-1}) were excited by the 532 nm line using a 2400 gr/mm grating. Raman spectra at high wavenumber range (between 3000 cm^{-1} and 4000 cm^{-1}) were excited by the 785 nm line using a 1200 gr/mm grating. Spectra were collected with six accumulations, each of 15 s.

Fourier Transform Infrared (FTIR) spectra were acquired on double-polished thin sections of 0.2 mm thickness using a Thermo Scientific Nicolet Centaurµs FT-IR Microscope operated via OMNIC software. Spectra were collected in the 1300–4000 cm^{-1} range, with 64 scans of sample exposure and 0.5 cm^{-1} of spectral resolution. The spatial resolution was 100 µm. The background spectra were run for 120 s before analysis and subtracted from the sample spectra.

Pseudotachylyte glass was analysed by micro-single-crystal X-ray diffraction using the Rigaku-Oxford Diffraction Supernova diffractometer at the Dept. of Geosciences, University of Padova. The diffractometer is equipped with an X-ray micro-source (wavelength MoKα) and a 200 K Pilatus detector (Dectris) performing 0–360° phi scan rotation with an exposure time of 120 seconds per degree. The beam spot was 0.12 mm and the sample-to-detector distance was 68 mm.

3. The Moncuni and Lanzo ultramafic massif

Lanzo is the largest (150 km^2) ophiolitic, ultramafic massif within the stack of metamorphic units (nappes) of the Western Alps. At the regional scale, the Lanzo massif largely consists of preserved spinel-bearing peridotites, enriched in plagioclase by melt impregnation, cut by oceanic gabbro dykes and wrapped by oceanic serpentinite mylonites (Bodinier, 1988; Kaczmarek and Müntener, 2008; Debret et al., 2013) (Fig. 1a). The transition from peridotites to foliated serpentinites is marked by strongly serpentinized meta-peridotites. Serpentinization of the Mesozoic Tethyan oceanic mantle is mostly related to hydration by seawater. The oceanic serpentine (lizardite) reacted pervasively to antigorite during subsequent Alpine subduction (Debret et al., 2013). During subduction, the serpentinized peridotite developed metamorphic olivine + antigorite after serpentinized mantle olivine, and zoisite + garnet + chloritoid + chlorite after plagioclase. In hydrated gabbros, eclogite-facies metamorphism caused the replacement of igneous plagioclase by jadeite + zoisite + garnet + kyanite, of olivine by talc + tremolite + chloritoid and of clinopyroxene by omphacite (Kienast and Pognante, 1988; Pelletier and Müntener, 2006; Scambelluri et al., 2017). The peak P-T conditions of eclogite-facies metamorphism have been estimated to be 600 °C and 2.1 GPa (Scambelluri et al., 2017: their Supplementary Fig. S18).

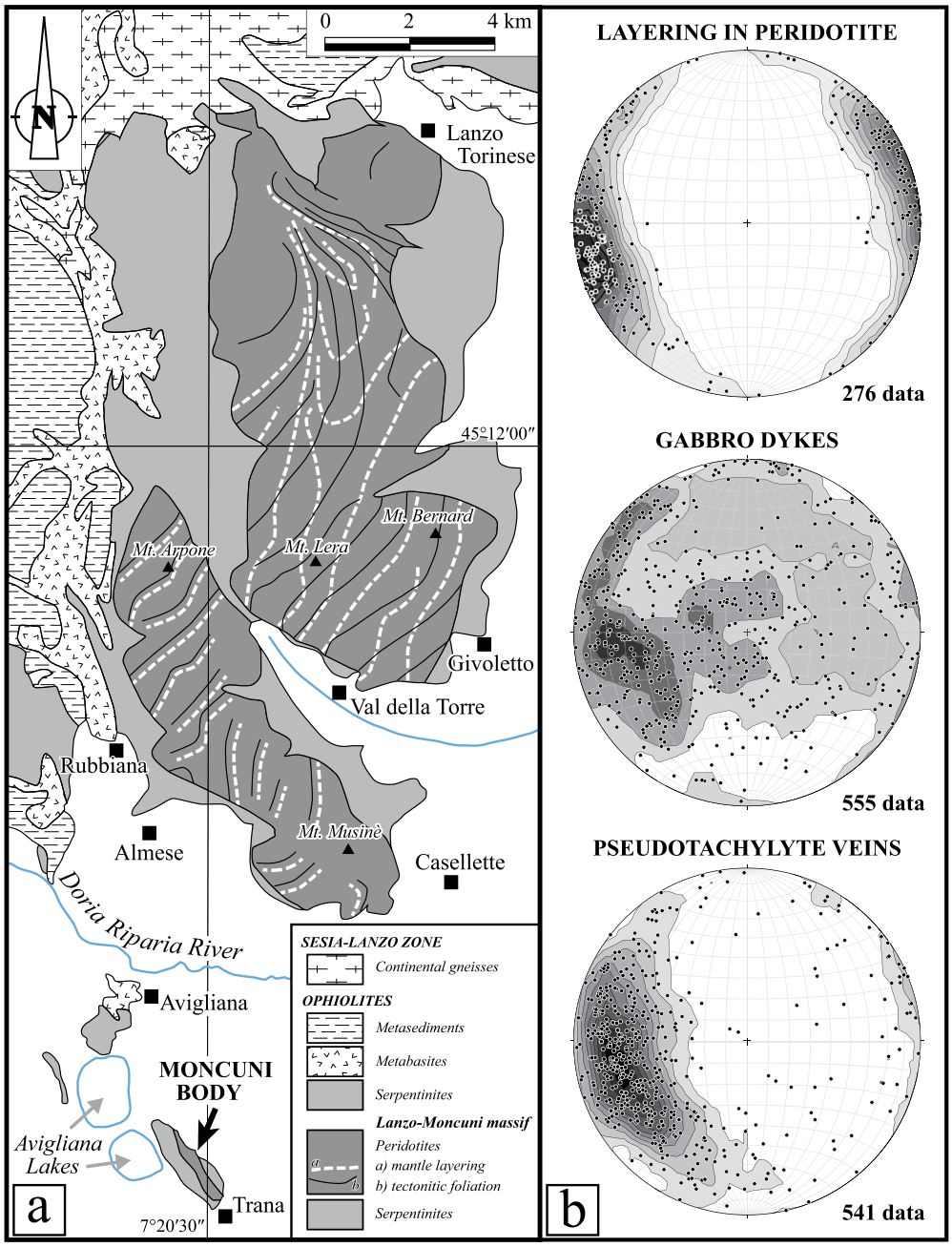

Fig. 1. (a) Geological sketch map of the Lanzo-Moncuni Ultramafic Massif and the surrounding Alpine units (modified from the compilation map of Kaczmarek and Müntener, 2008). (b) Orientations (equal area, lower hemisphere stereoplots) of the mantle layering, gabbro dykes and pseudotachylyte veins in the Moncuni body.

The gabbro–peridotite suite of the Moncuni ophiolite (the southernmost body of the Lanzo Ultramafic Massif: Fig. 1a) is volumetrically dominated by freshly preserved peridotite exhibiting a steeply-dipping, NNW-SSE-striking mantle tectonite foliation and pyroxenite layering (Fig. 1b). This peridotite fabric is cut by gabbro dykes (commonly a few cm in thickness). The dykes have a more scattered orientation, but still show clustering towards a NNW-SSE strike and moderate-steep ESE dip (Fig. 1b). The peridotite and gabbro are locally overprinted by mylonitic deformation, preferentially localized to the gabbro dykes (Fig. 2a–b). The mylonites and the magmatic-tectonite structures are commonly overprinted by brittle deformation (Piccardo et al., 2007; Scambelluri et al., 2017) (Fig. 2c), which is manifested by sharp micro-faults, thin (< 1–2 cm) cataclasite layers and pseudotachylyte veins. Altogether, the brittle structures form a complex network that is either concordant to the layering of peridotite and the prevailing set of gabbro dykes or crosscuts the layering and dykes (Fig. 2d). Pseudotachylytes are prominent in the peridotites (Fig. 2e) with veins reaching 40 cm in thickness. Within the gabbros, the pseudotachylyte veins are typically a few mm in thickness and only recognizable in polished slabs and thin sections, except for rare, cm-thick veins (Fig. 2f). Our study focuses on the clinopyroxene-plagioclase-olivine gabbros which are very similar in mineral composition to the host impregnated peridotites. The field-scale deformation structures within the gabbros are much more easily visible than those found in the peridotites. The Moncuni gabbros show nearly identical deformation features as the host peridotite. Thus, here we focus on the gabbros to make more general inferences on the rheology of a subducting oceanic slab.

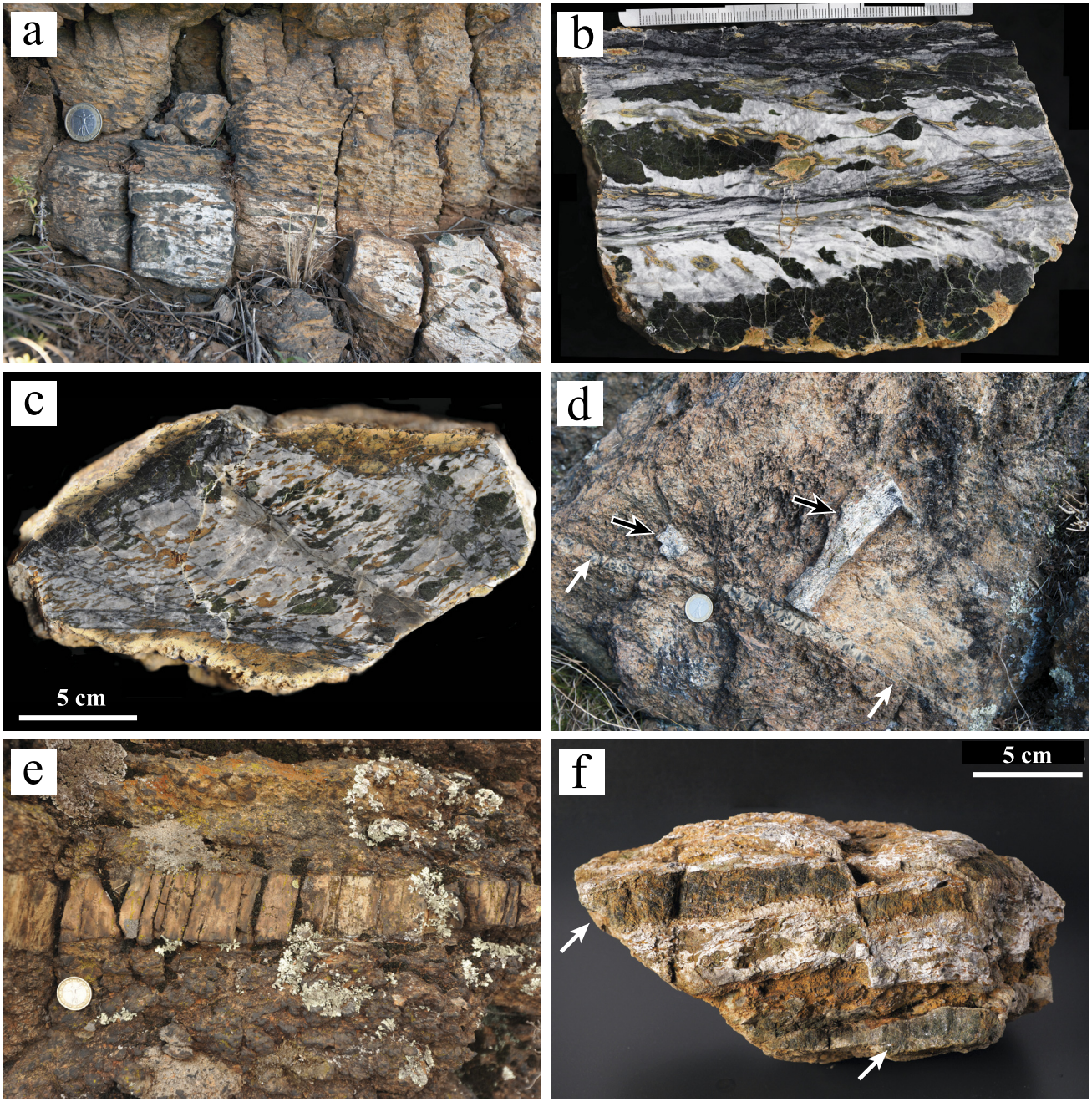

Fig. 2. Mesoscale structures of the Moncuni gabbros/peridotites: (a) Mylonitic foliation affecting a gabbro dyke and the bounding host peridotite. In the upper part of the photograph, the peridotite preserves the mantle fabric and layering. Coin scale 2.3 cm. WGS84 GPS location: 45.050002°N, 7.409973°E. (b) Polished slab of a heterogeneous ductile shear zone exploiting the core of a gabbro dyke. Note the coronitic static rims, due to eclogite-facies replacement, surrounding olivine (orange colour). Sample 16-14. WGS84 GPS location: 45.047559°N, 7.412997°E. (c) Gabbro dyke displaying a proto-mylonitic foliation, at a high angle to the dyke boundaries (upper and lower sides of the sample), and 2 sets of overprinting brittle structures that include: (i) a cm-thick cataclasite (left side of the sample), subparallel to the foliation and offsetting the dyke boundary; and (ii) thin cataclastic micro-faults, subparallel to the dyke boundaries. The greyish haloes of the micro-faults correspond to domains of brittle damage. Sample 15-114B. WGS84 GPS location: 45.049044°N, 7.410229°E. (d) Gabbro dykelet (indicated by black arrows) displaced by pseudotachylyte-bearing faults (a thick pseudotachylyte is indicated by white arrows) within peridotite. Coin scale 2.3 cm. WGS84 GPS location: 45.050001°N, 7.410035°E. (e) Thick pseudotachylyte, with the characteristic set of spatially dense joints orthogonal to the boundary, within peridotite. Coin scale 2.3 cm. WGS84 GPS location: 45.048250°N, 7.412919°E. (f) Thick, glassy pseudotachylyte (white arrows) within foliated gabbro. Sample 16-01 (loose block). WGS84 GPS location: 45.049389°N, 7.410033°E. (For interpretation of the colours in the figure(s), the reader is referred to the web version of this article.)

4. Deformation of the Moncuni gabbros

4.1. Oceanic mylonitic deformation

The magmatic assemblage of the gabbros consists of cm-sized sub-idiomorphic clinopyroxene (cpx_1), typically with exsolution lamellae of orthopyroxene (opx_1), idiomorphic plagioclase (pl_1), and olivine (ol_1). The igneous structure is commonly overprinted by a solid-state deformation that, at mylonitic stages, results in a mm-thick compositional layering (Fig. 3a) of monomineralic, dynamically recrystallized aggregates of polygonal grains of cpx_2, ol_2 and pl_2 (Fig. 3b, c). At high strain, the monomineralic aggregates start to disaggregate and undergo phase mixing by combined micro-boudinage/cavitation, exploiting grain boundaries, and nu-

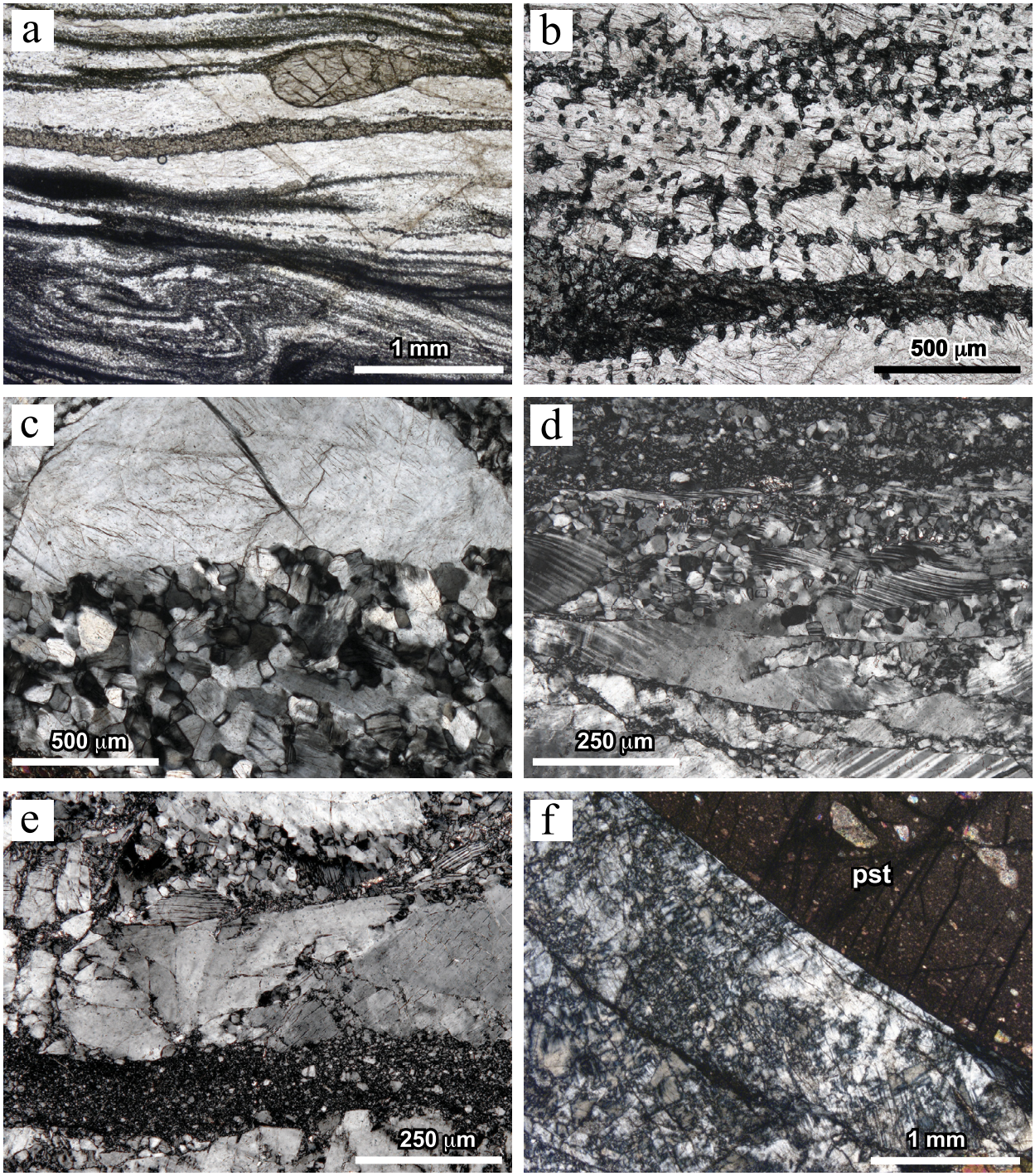

Fig. 3. Microstructure of gabbro mylonites. (a) Mylonitic foliation marked by a compositional banding of recrystallized *cpx*, *pl* and *ol*, involved in syn-mylonitic folding. In the upper part of the image, a recrystallized layer of *cpx* extends into the foliation from a relic magmatic porphyroclasts. Sample 16-235. (b) Incipient phase mixing between layers of recrystallized *ol* and *pl* in a mylonite. Sample 15-110. (c) Magmatic plagioclase (pl_1) dynamically recrystallized to a mosaic aggregate of dynamically recrystallized grains. Sample 15-110. (d) Magmatic and recrystallized plagioclase disrupted along brittle slip planes and cataclastic bands. Sample 15-111. (e) Ultracataclasite band crosscutting a partially recrystallized magmatic plagioclase. Sample 15-111. (f) Pervasive shattering of plagioclase in contact with pseudotachylyte (*pst*). Sample 15-07.

cleation of exotic grains of the bounding layer into dilatant sites (Fig. 3b).

4.2. Brittle deformation

Subparallel, sharp micro-faults and cataclasite layers, up to a few centimetres thick, pervasively affect the gabbros (Fig. 3d–e). Cataclasites record different episodes of deformation (Supplementary Fig. S1a) and are cut by different generations of pseudotachylyte veins (Supplementary Fig. S1b). Adjacent to micro-faults, cataclasites and pseudotachylytes, the host-rock minerals show pervasive brittle damage, as emphasized by the highly heterogeneous extinction of *pl* and *ol* and by bending of *cpx* crystal structure, transitional to domains of ultrafine comminution (Fig. 3f, Supplementary Fig. S2). This host-rock damage commonly occurs *in-situ*, without shear displacement of fractured grains. EBSD maps of cataclastic gabbro domains reveal, for all mineral phases, a very irreg-

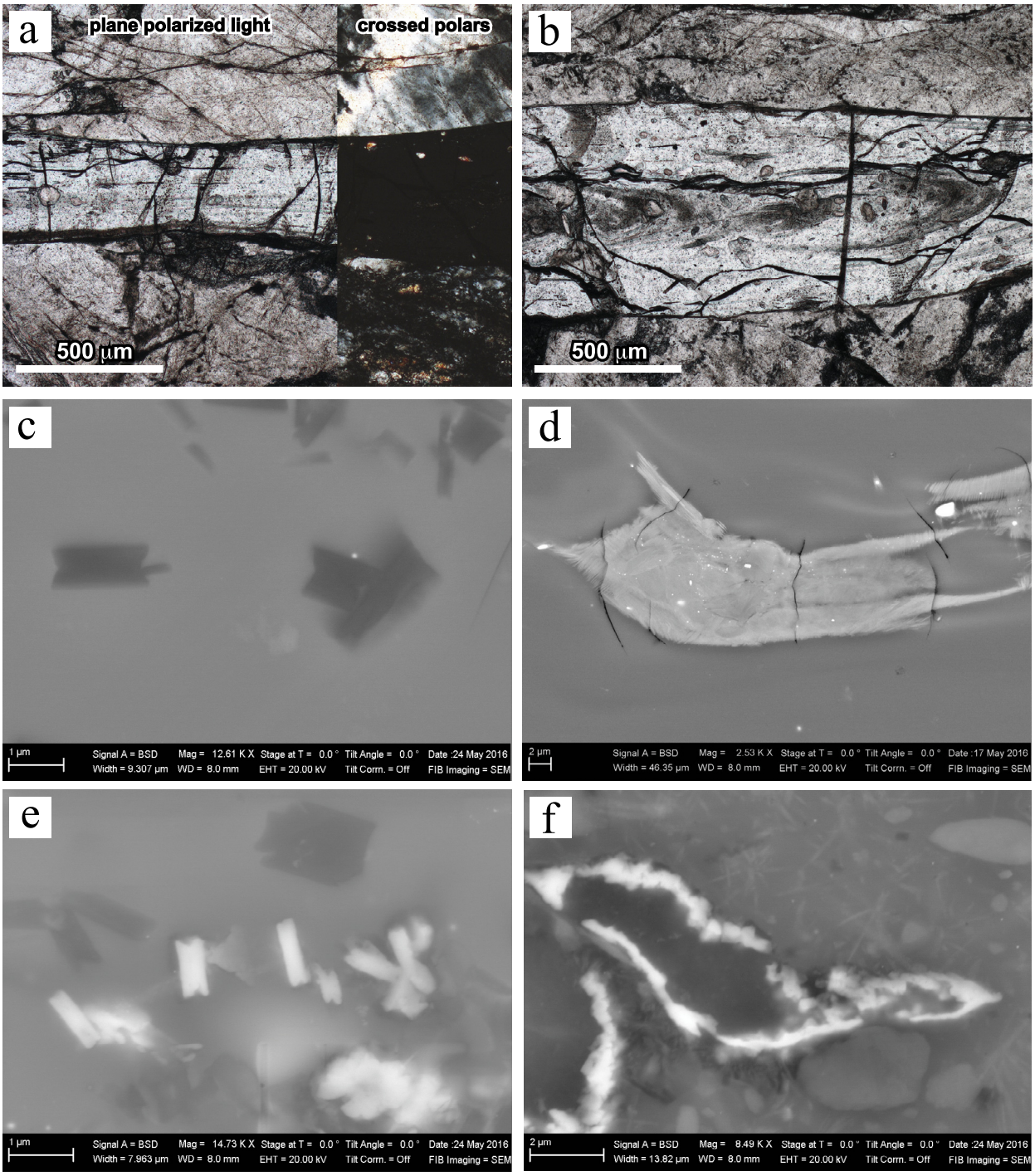

Fig. 4. Microstructure of thin pseudotachylyte veins. (a) Pseudotachylyte fault vein made of optically transparent (left: plane-polarized light) and isotropic (right: crossed polars) glass showing internal thin flow lines subparallel to the vein boundary. Sample 15-111. (b) Glassy pseudotachylyte vein with internal flow fold. Plane polarized light. Sample 15-111. (c) Hourglass-shaped dark microlites of plagioclase within a homogeneous pseudotachylyte glassy matrix. SEM-BSE image. (d) Feather microlitic aggregate of clinopyroxene within pseudotachylyte glass. SEM-BSE image. (e) Garnet (bright) and plagioclase (dark) microlites with similar shape and size within homogenous pseudotachylyte glass. SEM-BSE image. (f) Garnet (bright) rim surrounding a plagioclase clast in the pseudotachylyte glass.

ular grain size distribution and the absence of crystallographic preferred orientations of grains within the cataclastic matrix (Supplementary Fig. S3). However, cataclasites include grain clusters or individual, intensely fractured clasts that still retain the same crystallographic orientation of the flanking magmatic mineral grains, reflecting the contribution of *in-situ* fragmentation to the formation of the comminution bands. The ultrafine-grained portions of comminution domains show a high degree of non-indexed Kikuchi patterns. There is no evidence for metamorphic breakdown of igneous and high-temperature minerals during the brittle overprinting.

Pseudotachylytes mostly occur as thin fault veins, up to a few 100 µm thick, showing local injection veins into the host-rock. The damaged host-rock adjacent to pseudotachylyte fault veins is dismembered by injection veins and included as clasts within the pseudotachylyte matrix (Supplementary Fig. S2). Thin pseudotachylyte veins commonly consist of optically transparent, isotropic

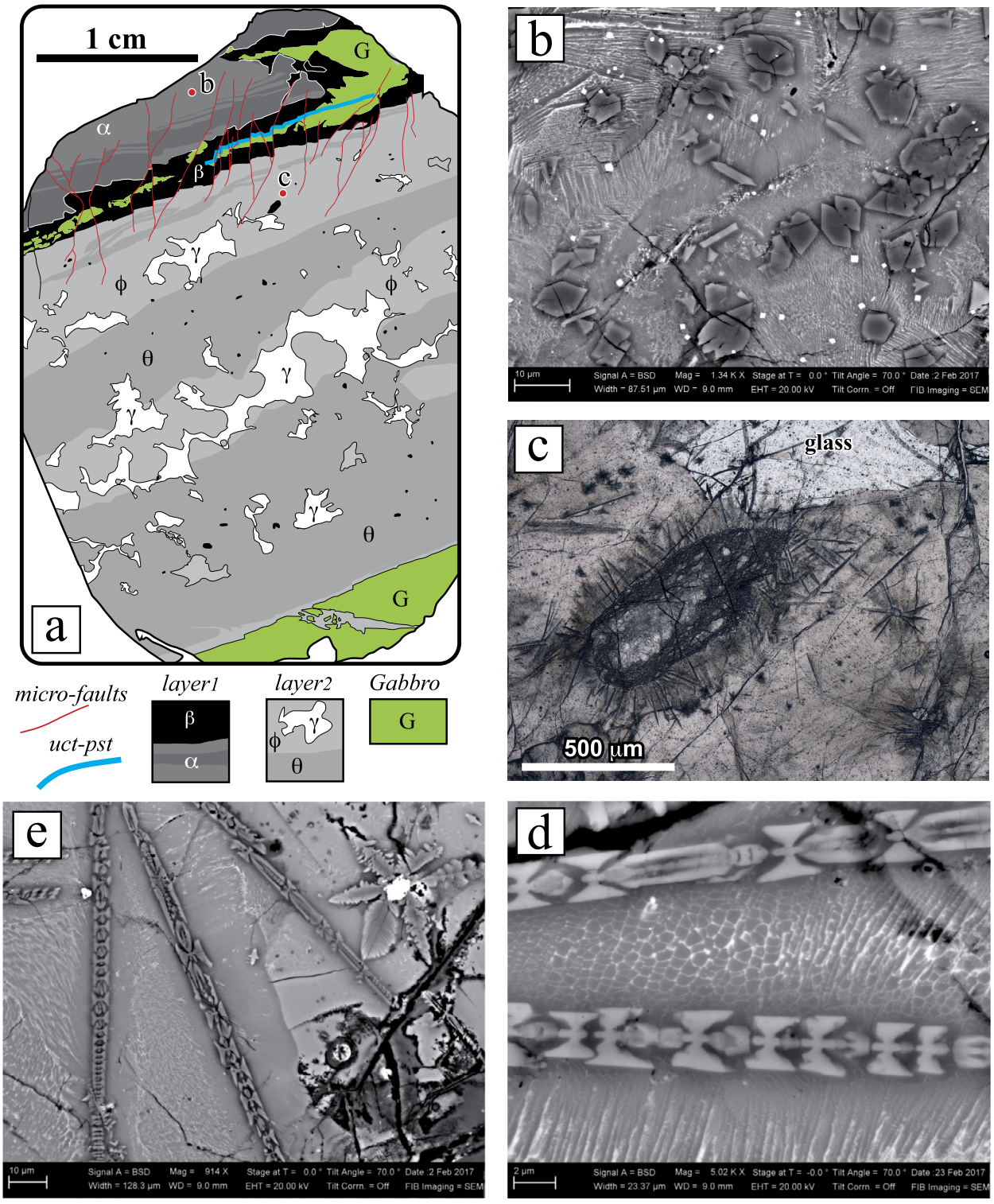

Fig. 5. Microstructures of thick pseudotachylyte vein (sample 16-401). (a) Sketch of the structure of a thin section of the sample 16-401. The thin section scan is shown in the Supplementary Fig. S4b. In $layer_1$, 2 different grey shades are used to highlight the internal layering of $layer_1\alpha$. In $layer_2$, θ and ϕ represent bands rich and free of chain olivine, respectively, scattered in the *cpx-pl* aggregate; γ represents residual glass patches. The few small clasts in $layer_2$ (black in colour) consist of olivine. (b) Granular olivine microlites within a matrix intergrowth of *cpx* (grey) and *pl* (light). SEM-BSE image. (c) Olivine clast (*ol*) surrounded by radially arranged needles of chain olivine set in a fine, brownish intergrowth of *cpx-pl*. At the top of the image a patch of transparent glass is preserved. Optical image in plane-polarized light. (d) Chain olivine (light grey) immersed in an intergrowth of *cpx* (light) and *pl* (darker grey). SEM-BSE image. (e) Chain olivine within a fine intergrowth of *cpx-pl* (left side of the photograph) and glass (right side). The glass contains a stellate *cpx* spherulites, radiating from spinel nuclei (bright). *Utc-pst*: ultracataclasite-pseudotachylyte. SEM-BSE image.

glass (as confirmed by Raman and X-ray diffraction) containing very few, minute clasts. The glass displays flow lines subparallel to the vein boundary, embayed in injection veins, and highlighting flow folds (Fig. 4a, b). Tiny microlites of prismatic *pl* (hourglass in shape: Fig. 4c) and acicular *cpx* (Fig. 4d) are locally present. In SEM-BSE images, the glass appears homogeneous or shows a fine compositional layering. Frequently these layers are clustered with micrometric clasts, delineating the flow structure. The dif-

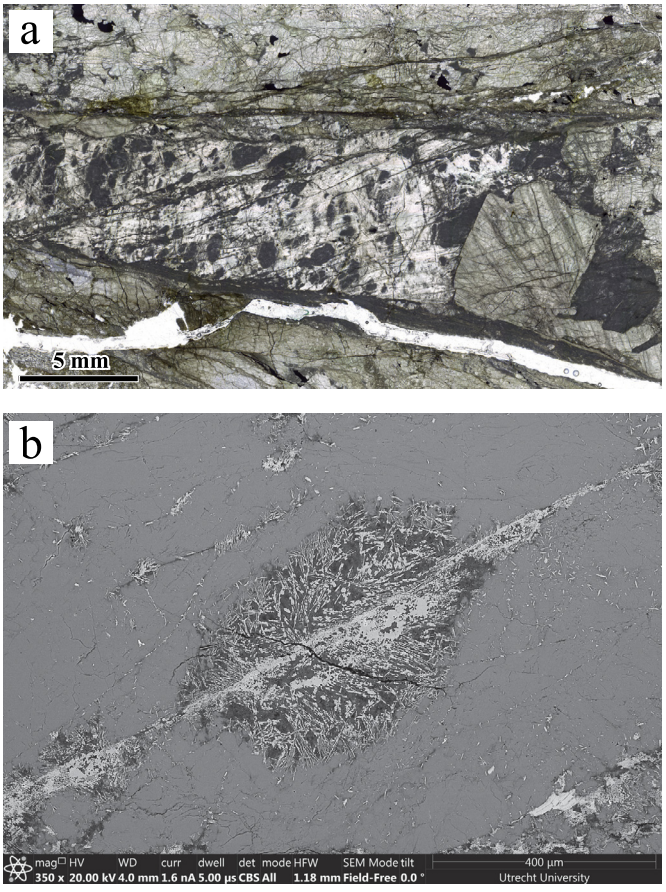

Fig. 6. Incipient post-seismic hydration. (a) Overview optical microphotograph (plane-polarized light) of a gabbro dykelet (central part of the photo) within peridotite. The gabbro consists of partially preserved plagioclase (white) and clinopyroxene (light green) showing extensive micro-fracturing. In the plagioclase the dark, locally globular-shaped areas correspond to domains altered to zoisite + paragonite. The ultracataclastic layers at the dykelet boundaries also show a dark appearance related replacement by eclogite-facies zoisite + paragonite ± garnet ± jadeite. The replacement is primarily restricted to brittle fractures in plagioclase and plagioclase-derived ultracataclasite, whereas the shattered clinopyroxene and the peridotite ultracataclasite escaped re-equilibration. (b) SEM-BSE image of eclogite-facies globular aggregate replacing plagioclase in the gabbro. This aggregate is linked to a precursor brittle microfracture also decorated by eclogite-facies reaction products.

ferent compositional layers locally show the incipient growth of either *pl* or *cpx* microlites. Garnet locally occurs as pseudomorphs of *pl* microlites (Fig. 4e), or as more irregular thin overgrowth of *pl* clasts (Fig. 4f).

Fig. 5a shows the thin section sketch of a 3.5 cm-thick pseudotachylyte (sample 16-401). In contrast with thin veins, this thick vein is largely crystallized to microlitic aggregates of *pl*, *cpx*, *ol* ± *opx*, though large patches of glass are still present in the vein core. The vein is texturally zoned and consists of two main composite layers (*layer*$_1$ and *layer*$_2$) whose microstructure is illustrated in detail in the Supplementary Fig. S4, and summarized here. *Layer*$_1$ is finer-grained and does not contain glass. In *layer*$_1$, olivine occurs either (*layer*$_1\alpha$ and less frequently in *layer*$_1\beta$) as granular idiomorphic microlites (< 10 µm grain size), with local hopper crystal habit, set into a fine intergrowth of fibrous *cpx* and *pl* microlites (10 s to 100 µm long) (Fig. 5b), or as interstitial grains together with *cpx* in an equigranular microlitic aggregate of prismatic *pl* (*layer*$_1\beta$) (Supplementary Fig. S4d). *Layer*$_1\beta$ includes numerous small clasts of gabbro minerals and a large shred of cataclastic gabbro, and is cut by a thin (ca. 10 µm) ultrafine cataclasite (Supplementary Fig. S4e).

Layer$_2$ predominantly consists of a fine aggregate of intergrown, fibrous *cpx* and *pl* microlites. This aggregate forms a palisade structure, at the layer boundary, and transitions to an aggregate of large (mm-long), randomly oriented microlitic sheaves and radiating spherulites in the vein core. Large (mm-sized) residual patches of optically transparent, isotropic glass occurs between the *cpx-pl* spherulites in the vein core (Fig. 5a, c; Supplementary Fig. S4h, j, k). The *cpx-pl* microlitic aggregate and glass include an internal composite substructure of subparallel clusters of: (i) microlitic granular *ol*, at a distance < 1 mm to the boundary to *layer*$_1$ (Supplementary Fig. S4f); and (ii) sparse, randomly oriented chain *ol* (Fig. 5c–e; Supplementary Fig. S4g–h), locally arranged radially around *ol* clasts (Fig. 5c). Small stellate *opx* spherulites, radiating from spinel nuclei (few µm in diameter) (Fig. 5e; Supplementary Fig. S4i), are scattered throughout *layer*$_2$. The occurrence of chain *ol*, and of the large glass patches are the main distinguishing features of *layer*$_2$ compared with *layer*$_1$ and, together with the coarser grain size of the microlitic *cpx-pl* aggregate, likely reflect slower cooling rates.

The thick veins of sample 16-01 displays a similar microstructure as *layer*$_2$ of sample 16-401 with a dominant glassy matrix locally overgrown by *cpx* and *pl* spherulites (Supplementary Fig. S5a). Also, the microstructure is crosscut by a new generation of glassy pseudotachylyte, subparallel to the vein boundary, showing marked flow structures (Supplementary Fig. S5b).

5. Development of hydrous assemblages

In the Moncuni gabbros and peridotites, the cataclasites and pseudotachylytes locally either overprint or are crosscut by the eclogite-facies hydrous assemblages (Scambelluri et al., 2017). Fig. 6 shows the static overgrowth of zoisite + paragonite ± garnet ± jadeite partially replacing the fractured magmatic plagioclase of a gabbro dykelet and extensively overgrowing the ultracataclasite at the boundary with the host peridotite. In the plagioclase, this eclogite-facies replacement is spatially linked to the crosscutting micro-faults. The micro-faults themselves are decorated by the eclogite-facies breakdown products (Fig. 6b). In general, where present, the incipient development of eclogitic assemblages is typically associated with the brittle deformation microstructures. The hydrous eclogite-facies aggregates never display a strain-induced foliation even where the degree of replacement of the pre-existing minerals is extensive.

6. Mineral composition and temperature of oceanic mylonitization

The Moncuni gabbros consists of (Cr, Al, Na)-bearing diopsidic clinopyroxene (*cpx*$_1$) [Mg/(Mg+Fe)$_{mol}$ = 0.88–0.91], Forsterite$_{87–89}$ olivine (*ol*$_1$) and Anorthite$_{59}$ plagioclase (*pl*$_1$). Exsolution lamellae of orthopyroxene (*opx*$_1$) in *cpx*$_1$ have an enstatitic composition [Mg/(Mg + Fe)$_{mol}$ = 0.84–0.88]. The chemical compositions of the magmatic minerals are reported in the Supplementary Table 1.

In the gabbro mylonites the recrystallized *cpx*$_2$ is less (Cr, Al, Na)-rich than the igneous *cpx*$_1$. *Pl*$_2$ has a more variable composition (An$_{47–69}$Ab$_{53–31}$) than *pl*$_1$ (Supplementary Table 2). *Cpx*$_2$-rich aggregates contain very minor pargasitic amphibole and chromian spinel ($Mg_{0.54}Fe^{2+}_{0.45}Al_{0.93}Cr_{0.90}Fe^{3+}_{0.15}O_4$), and less abundant orthopyroxene (*opx*$_2$). *Opx*$_2$ is slightly less (Cr, Al)-rich than the *opx*$_1$ lamellae in the *cpx*$_1$ porphyroclasts.

The temperatures of mylonitic deformation were estimated by pyroxene geothermometry. Independent single-clinopyroxene (Nimis and Taylor, 2000) and single-orthopyroxene (Brey and Köhler, 1990) thermometers were used in order to check for chemical equilibrium between coexisting pyroxenes. The *Ca-in-opx* estimates were corrected (Nimis and Grütter, 2010) in order to make up for

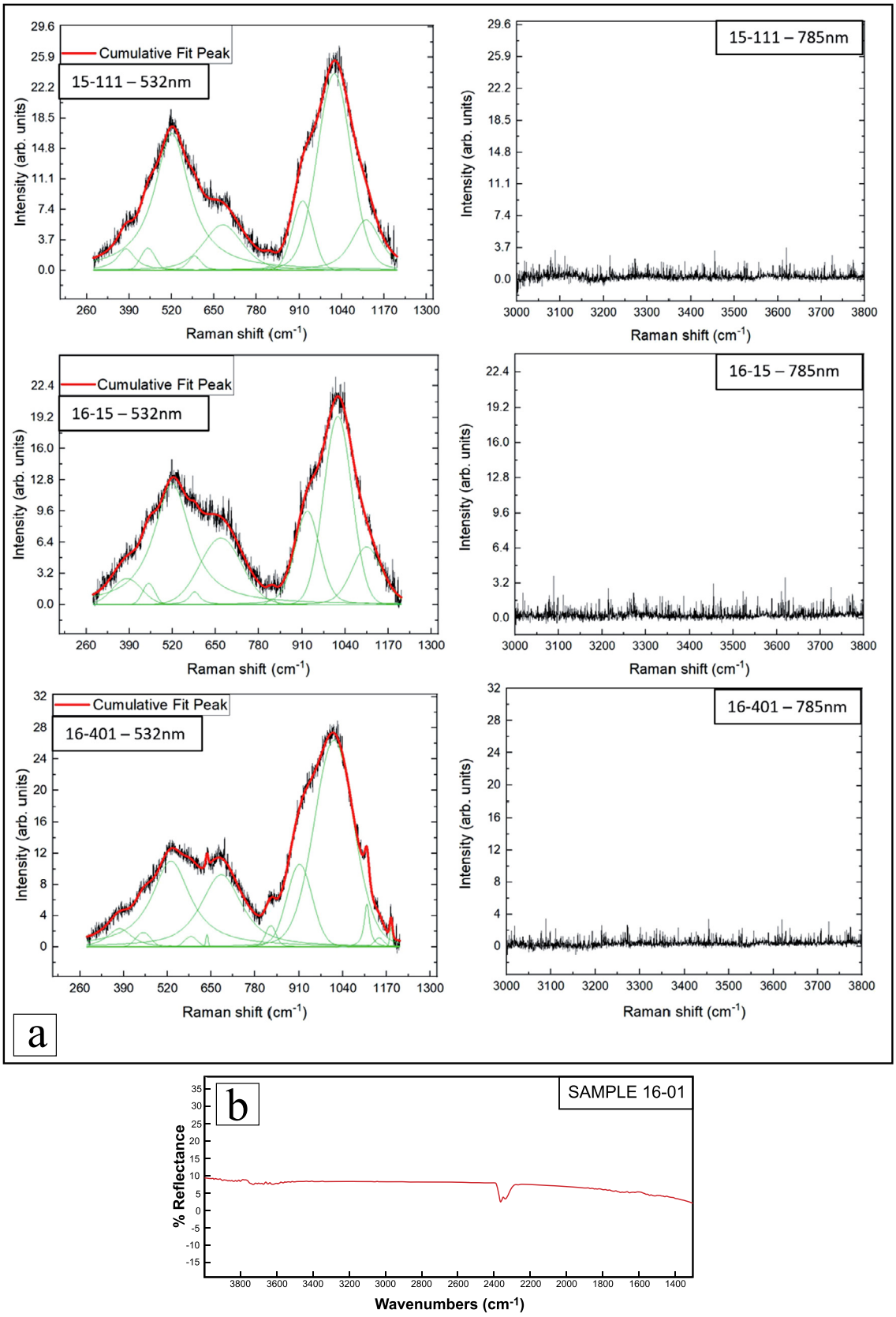

Fig. 7. Raman (a) and FTIR (b) spectra of pseudotachylyte glass.

recognized inconsistencies between the two geothermometers at low temperatures. The temperatures estimated (at a nominal pressure of 0.3 GPa) for cpx_2 and opx_2 from the same microstructural domain differ by 16–49 °C, suggesting local equilibrium. These temperatures lie in the range of 763–820 °C (mean = 775 °C). Exsolved cpx_1 and the included opx_1 lamellae yield largely overlapping estimates (712–807 °C; mean = 761 °C). No systematic difference is observed between temperature estimates for cpx_1 and cpx_2 from the same microstructural domain.

7. Pseudotachylyte glass composition and water content

X-ray diffraction measurements show that the optically isotropic, transparent matrix of pseudotachylyte is amorphous glass (Supplementary Fig. S6). Consistently, all measured Raman spectra show three main peaks at 520, 685 and 1000 cm^{-1}, typical of basaltic glasses (Di Muro et al., 2006, 2009). The glass filling the thin veins (Figs. 2c and 4) displays marked compositional variations (Supplementary Table 3) and is characterized by the absence, or by rare, tiny microlites. Thin pseudotachylytes show a trend of progressive Al-enrichment and Mg-depletion departing from the bulk composition of the olivine gabbros (Supplementary Fig. S7). Differently, the residual glass patches of thick pseudotachylytes (Figs. 2f and 5), which show extensive crystallization of microlitic plagioclase-clinopyroxene intergrowths and only minor olivine, are enriched in Mg with respect to the bulk rock geochemistry of the gabbro.

The water content in the pseudotachylyte glass was evaluated by Raman analysis on two thin pseudotachylyte veins (samples 15-111 and 16-15) and one thick pseudotachylyte vein (sample 16-01). In the high wavenumber range (3000–4000 cm^{-1}) the spectra do not show any peak (Fig. 7a). The Raman spectra are indicative of dry glass composition (Di Muro et al., 2009) because they lack OH-stretching vibrations at wavenumbers in the region around 3500 cm^{-1}. Because of the large beam size, only the mm-sized glass patches from the thick pseudotachylyte vein (sample 16-01) were suitable for FTIR measurement. In unison with the Raman results, the measured FTIR spectra (Fig. 7b) do not show any absorption bands in the wavelength region between 3000 and 4000 cm^{-1} that would be indicative of OH-species. The absence of significant absorption band in the region around 1650 cm^{-1}, where the H_2O bending vibration is expected, also excludes any subsequent glass alteration.

8. Discussion

8.1. Metastability and water-absent conditions of Moncuni ophiolites

The high-temperature (~ 750–800 °C) mylonitic fabrics, developed in the gabbros and in the host mantle peridotite prior to subduction, are well preserved in the core of the Moncuni body. These fabrics remained mostly unaffected by ductile deformation and metamorphism during subsequent subduction but were pervasively overprinted by brittle deformation events (cataclasis, frictional melting and *in-situ* fragmentation). This excludes the occurrence of self-localizing thermal-runaway (Kelemen and Hirth, 2007; John et al., 2009) for the development of the Moncuni pseudotachylytes. Metamorphic replacement of the pre-subduction minerals is absent even in domains of stronger brittle deformation. In the subordinate serpentinized peridotites and the metagabbros, the pseudotachylytes and the micro-faults both pre-date and post-date the eclogite-facies minerals statically replacing the pre-subduction minerals (Scambelluri et al., 2017). This attests that coseismic brittle structures experienced subduction conditions of ~ 600 °C and > 2 GPa.

The resistance to metamorphic re-equilibration and ductile deformation can be explained by water-absent conditions. Dry conditions persisted throughout the whole Alpine cycle of subduction and exhumation of the Moncuni ophiolite. The dry composition of the protolith, which contained very minor amphibole as exsolution lamellae in clinopyroxene, is corroborated by the dry composition of the pseudotachylyte glass, as well as by its exceptional preservation. Water-absent conditions are further confirmed by widespread preservation of anhydrous, pre-subduction minerals in the cataclasites and fragmented domains. If hydrous fluids were present, the pervasive cataclastic network would have provided high-permeability pathways for fluid infiltration, leading to much more extensive metamorphic re-equilibration than observed in our samples (Fig. 6).

Studies of the exhumed continental, lower crustal granulites of Holsnøy in the Bergen Arcs, Norway (e.g. Jamtveit et al., 2018), propose that propagation of deep earthquake ruptures (recorded by pseudotachylytes) into these dry, metastable, stiff rocks promoted fluid infiltration along the permeable fault cores and damage zones, causing transformation of dry granulites into hydrous eclogites. Hydration and metamorphic re-equilibration of granulites induced mechanical weakening and favoured the development of the regional pattern of eclogite-facies ductile shear zones (Austrheim, 2013). In contrast to the Holsnøy rocks, the Moncuni ophiolite remained unaffected by massive fluid influx along the pervasive seismic brittle deformation zones. On a regional scale, the dry rocks of Moncuni and Lanzo are encompassed by serpentinite shear zones. Early serpentinization (lizardite) of the Lanzo lithosphere occurred in a slow-spreading ridge, oceanic context (Debret et al., 2013). During subduction, antigorite replaced lizardite and then underwent partial breakdown to olivine + water at peak eclogite-facies conditions. The amount of water released by the partial breakdown of antigorite mainly remained confined within the serpentinites, producing a sharp boundary between serpentinites and peridotites which corresponds to the original oceanic serpentinization front (Debret et al., 2013). Therefore, antigorite dehydration was insufficient (or water was efficiently removed by a dominant upward flow in the slab: e.g. Plümper et al., 2017) to promote significant hydration and eclogitization of the faulted domains in the Moncuni and Lanzo bodies.

8.2. Thermal threshold for ductile deformation of dry oceanic lithosphere

In the absence of aqueous fluids, dry crystalline rocks, such as peridotite and gabbro, are expected to resist without experiencing ductile flow up to high metamorphic grade. Several studies of the Holsnøy area, Norway, have well documented that dry lower crustal granulite is capable of metamorphically reacting and flowing under eclogite-facies conditions when hydrated by infiltrating fluids. The Moncuni rocks show that dry oceanic peridotites and gabbros were prone to flow at ~ 750 °C: below this temperature such rocks escaped ductile deformation and were characterized by negligible reaction kinetics even at submicron scale. Pinpointing this thermal threshold is relevant to interpret the fate of the oceanic lithosphere during subduction and its tectonic incorporation as ophiolitic fragments into orogenic accretionary wedges at subduction margins. The peak temperatures recorded by subducted units now exposed in the Alpine orogen (including ultrahigh-pressure units) are in the range of ~ 550–650 °C (Agard et al., 2009). The vast majority of Alpine ophiolites includes extensively serpentinized peridotites which, together with hydrated mafic bodies, were strongly affected by metamorphism and ductile deformation under high-pressure conditions (Angiboust et al., 2011; Deschamps et al., 2013; Scambelluri et al., 2019). Also in low strain domains, coronitic reactions or pseudomorphic replace-

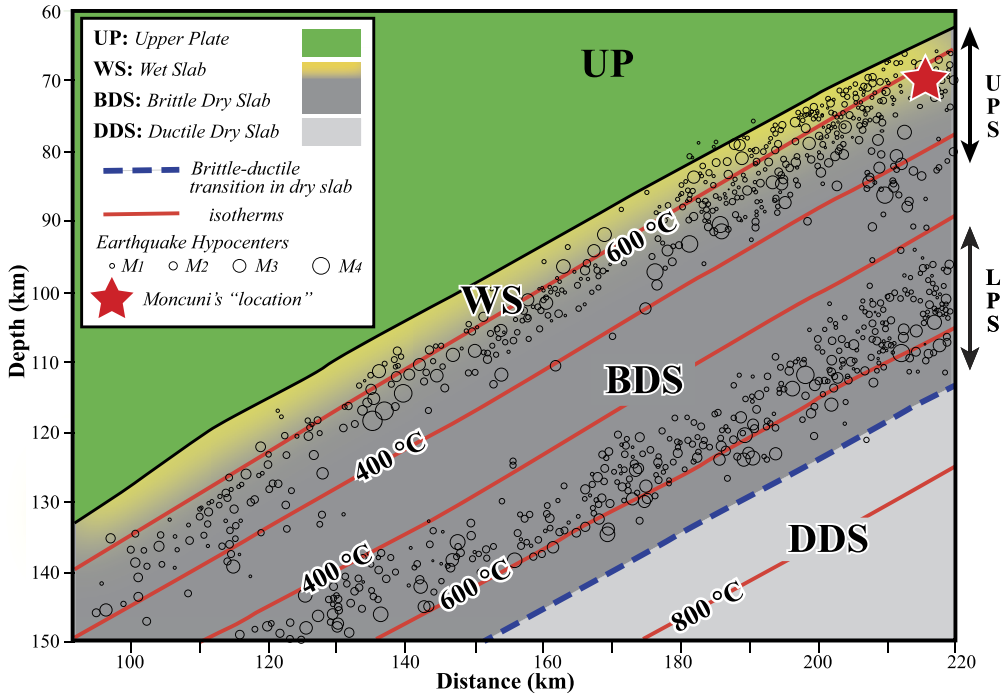

Fig. 8. Conceptual model of the rheology of a subducting oceanic slab overlap on the scheme of earthquake distribution in the subducting slab of Japan redrawn and modified from Kita et al. (2006) and Yamasaki and Seno (2003).

ment of the pristine mantle/oceanic minerals are pervasive to complete, indicating an evolution in water-rich environments throughout the oceanic, subduction and exhumation histories (Barnicoat and Cartwright, 1997; Gilio et al., 2019). These features suggest that most Alpine ophiolites originated from the uppermost, hydrated portions of the oceanic lithosphere. These portions were more favourably incorporated and exhumed within the orogenic accretionary prism. The dry, metastable and undeformed lithosphere exposed at Moncuni and Lanzo is a rare relic of the rigid portions of the oceanic lithosphere from the upper part of the slab below the hydration front. This part is primarily lost by subduction and is thus under-represented in the exhumed metamorphic ophiolites of the Alpine orogenic stack.

8.3. The Moncuni ophiolite as a proxy for the origin of intermediate-depth seismicity

The brittle structures presented here are the result of coseismic deformation that produced extensive damage and fragmentation of the rock domains bound to pseudotachylyte fault veins. A comparable association of pulverized rocks and pseudotachylytes has been observed in the lower crustal granulites on Holsnøy and attributed to coseismic off-fault damage during propagation of an earthquake rupture (Petley-Ragan et al., 2019). Moreover, coseismically pulverized rocks have also been produced in high-pressure experiments (Incel et al., 2019).

The Moncuni (and Lanzo) peridotite and gabbro section is a dry remnant of the Tethyan oceanic lithosphere underlying the km-thick package of hydrated crust and serpentinized mantle formed by seawater-rock interaction in a slow-spreading ridge. The Lanzo serpentinites inherit the original thickness of the altered layer atop the oceanic lithosphere (Debret et al., 2013). The intermediate-depth subduction earthquakes recorded at Moncuni thus occurred within the "upper plane" of seismicity (UPS) of the double seismic zone (Umino and Hasegawa, 1975; Kawakatsu, 1985), not distant from the subduction interface (Fig. 8; see also Scambelluri et al., 2017). Moreover, the mechanical behaviour recorded by the Moncuni peridotite section may also be a proxy of intra-slab seismicity along the LPS located 15–30 km below the UPS. The LPS domains of the oceanic slab are never exhumed to the Earth's surface and sink into the mantle.

The LPS is characterized by low seismic wave velocities and low V_p/V_s, which have been related to the presence of fluids and/or serpentinized mantle domains. Considering this, the LPS earthquakes have been explained by a mechanism of dehydration embrittlement due to serpentine breakdown (Seno and Yamanaka, 1996; Peacock, 2001; Yamasaki and Seno, 2003). This model is supported by the fit between the base of the LPS with the expected, nearly isothermal conditions of serpentine dehydration (in the range between 600 and 800 °C) (Yamasaki and Seno, 2003). This commonly-held view is contrasted, however, by the poor evidence for the presence of serpentinite at 15–30 km depth in oceanic plates and by the fact that faulting and serpentinization are likely limited to shallow depths at both mid-oceanic ridges ($<$ 17 km in ultra slow-spreading ridges: Grevemeyer et al., 2019), and at the trench–outer rise systems ($<$ 15 km for faulting related to slab bending: Ranero et al., 2003; Faccenda, 2014; Faccenda et al., 2009). Other authors have suggested that fluid can deeply percolate along thermal cracks forming in the oceanic lithosphere down to 30 km after 100 Myr of cooling (Korenaga, 2017). However, the deepening of fluid percolation and serpentinization should be associated with continuous hydrothermal activity, which is not observed in old ($>$ 65 Myr) plates (Stein and Stein, 1994) where, according to thermo-elastic modelling, thermal crack growth is limited to 20 km. In addition, the hydrated thermal cracks have not been detected by geophysical surveys, hence remaining a potential, but an unconstrained tectonic feature. Redistribution of water stored within slab serpentinites during the prograde subduction path and plate unbending (Faccenda et al., 2009; their Fig. 18) is at odds with (i) the lack of pervasive hydrated mineral assemblages or microstructures related to fluid infiltration within the Moncuni peridotite, and (ii) the fact that the UPS and LPS are separated by a layer with high seismic velocities typical of pristine dry peridotite. An alternative suggestion is that the low seismic velocities and low V_p/V_s at LPS result from the seismic anisotropy produced by hor-

izontal shear zones and faults in dry peridotite (Reynard et al., 2010). This latter interpretation is supported by our observations from the Moncuni rocks indicating that dry oceanic peridotite/gabbro experienced ductile flow at temperatures $\geq$ 750–800 °C, i.e. at the same temperature conditions expected for serpentinite dehydration. The lower cut-off of LPS seismicity can, therefore, be viewed as a temperature-dependent brittle-ductile transition inside the dry oceanic slab mantle, rather than a dehydration boundary in altered mantle domains. Overall, the same thermal threshold can be valid to explain seismicity in an oceanic environment.

As schematized in Fig. 8, the rheological layering of a subducting oceanic slab at intermediate, eclogite-facies, depths may consist, from bottom to top, of (i) an aseismic dry and ductile mantle, (ii) a 15 to 30 km-thick rigid and dry mantle extending from the base of the LPS to include a conspicuous portion of the UPS, and (iii) a hydrated, ductile layer at the subduction interface (WS). In the Alpine nappe stack and in other collisional mountain belts, the hydrated seismic layer atop the slab is made up of hydrated ophiolitic units that are preferentially incorporated in the accretionary wedge and exhumed in the orogenic belt. For the Alpine subduction, in particular, the presence of such a hydrated layer is expected, considering the origin of the oceanic lithosphere at a slow-spreading ridge. From a seismic viewpoint, the slab architecture shown in Fig. 8 can thus be considered representative of the fossil Alpine subduction zone as well as of the present-day circum-Pacific subduction zone system. The WS accommodates deformation by dominant ductile flow, but undergoes transient episodes of brittle, fluid-assisted fracturing recorded by dehydration veins, filled with eclogite-facies minerals, and by eclogitic breccias (Locatelli et al., 2018). The fracturing and veining episodes are potentially consistent with seismicity associated with dehydration embrittlement. The transition of the WS to the underlying dry mantle corresponds to a gradual hydration front (Fig. 8), marked by a zone of dry peridotite pods embedded in serpentinite, which was in part already assembled in an oceanic slow-spreading ridge context. This transitional zone is represented by Lanzo-Moncuni massif and, presumably, by a few other examples (e.g. Alpine Corsica: Andersen and Austrheim, 2006; Fabbri et al., 2018).

Our observations suggest that dehydration embrittlement, associated with over-pressurized pore fluids, did not play a role in the Moncuni-Lanzo transitional zone. This finding may suggest fast and efficient removal of water, derived from dehydration within the WS, along dynamically evolving fluid pathways within serpentinite (Plümper et al., 2017). Only a minor fluid flow component infiltrated the damage zones of the seismic faults in peridotites (e.g. Fig. 6) to reach the underlying dry mantle. Seismicity in Moncuni can be referred to build-up of high differential stresses in dry peridotite driven by local dehydration of small scattered volumes of antigorite-rich bodies (Ferrand et al., 2017), or by local stress amplification due to jammed pods of dry peridotite in a serpentinite matrix (Beall et al., 2019). A more general trigger for seismic failure at both the UPS and LPS is the unbending of the rigid dry mantle layer (BDS in Fig. 8) confined between the upper hydrated zone at the subduction interface and the ductile dry mantle below the 700–800 °C isotherm. Triggering earthquakes under eclogite-facies conditions ($>$ 2 GPa) in dry rocks faces the problem of the ultra-high differential stresses necessary for brittle yielding. This same problem is encountered for lower continental crust earthquakes where conditions of pseudotachylyte formation have been estimated to 600–700 °C and 1.0–1.3 GPa (Musgrave Range, Central Australia: Hawemann et al., 2018), 650–750 °C and 0.7–0.8 GPa (Lofoten, Norway: Menegon et al., 2017), and $\sim$ 680 °C and 1.5 GPa (Holsnøy, Norway: Jamtveit et al., 2019). These exhumed rocks were dry and, in the case of Musgrave and Lofoten, remained dry after extensive coseismic brittle faulting, therefore, excluding a direct link with fluid infiltration. High differential stresses during formation of subduction-related pseudotachylytes in exhumed ophiolites (Lanzo and Alpine Corsica) or in the deep, dry lower continental crust are supported by the reported conspicuous volumes (compared with shallower geologic contexts) of pseudotachylytes reflecting highly energetic earthquakes. The occurrence of these energetic earthquakes nucleating in the dry UPS may induce the transient seismicity in the fluid-rich environment of the WS.

9. Conclusions

The dry peridotite and gabbro building up the oceanic lithosphere undergo ductile flow at temperatures higher than ca. 700 °C. At the peak subduction temperatures of 600 °C experienced by many exhumed eclogite-facies ophiolites, the dry oceanic lithosphere deforms by brittle/seismic faulting. Dry rocks likely form most of the subducting oceanic lithosphere in many cases, with the exception of the relatively thin hydrated layer atop the slab. Slices of this uppermost hydrated layer are most easily scraped off the slab, incorporated in accretionary wedges or along the subduction plate interface and entrained as ophiolitic tectonic units in collisional belts. Such ophiolites are commonly strongly mylonitised and re-equilibrated at synkinematic metamorphic conditions during the subduction and exhumation paths, even at relatively lower temperatures.

In contrast, the subducted dry oceanic lithosphere is only rarely exposed. The Moncuni ophiolites presented here thus provide an exceptional geological record of the rheology and intermediate-depth subduction seismicity of a dry lithospheric slab. Under eclogite-facies conditions the Moncuni lithosphere neither yielded ductilely nor extensively recrystallized to high-pressure subduction assemblages. Instead, these dry rocks failed by seismic faulting recorded by extensive pseudotachylytes. Extreme dry conditions of the Moncuni rocks are testified by the preservation of the eclogite-facies pseudotachylyte glass across subduction and exhumation. Our study confirms that the accessibility of aqueous fluids has a first-order control on creep deformation and metamorphic reactions. The dry rocks of Moncuni were proximal to extensively serpentinized mantle, dehydrating at eclogite-facies conditions, but there is no evidence for significant fluid percolation along the spatially dense, damage zones associated with seismic faulting.

The Moncuni pseudotachylytes record that seismicity in the UPS can be driven by the failure of the dry portions of the oceanic slab near to, or entrained in, the low-velocity zone. The seismic structures shown here also provide a snapshot of LPS seismicity within the slab interior, suggesting that the base of the LPS within the subducting dry oceanic lithosphere corresponds to the thermally-controlled brittle-ductile transition.

Author contributions

G.P. and M.S. conceived the idea. G.P., M.S. and L.N. undertook data collection during fieldwork, and the petrographic and microstructural analysis. M.B. performed the BSE-SEM analysis and imaging, and elaborated the EBSD data. L.N. collected the Raman spectra. L.N and O.P. collected the EBSD data. P.N. performed the EMPA analysis and applied the single-pyroxene thermometry. L.N. and G.P. collected the EMPA glass composition. F.N. collected and elaborated the FTIR and single X-ray diffraction data. M.F. contributed on the discussion of the rheology of subducting oceanic slab and the role of water during intermediate-depth earthquakes. G.P. wrote the manuscript draft and all co-authors contributed to writing and revision.

Declaration of competing interest

The authors declare that they have no known competing financial interests or personal relationships that could have appeared to influence the work reported in this paper.

Acknowledgements

G.P. acknowledges funding from the University of Padova (BIRD175145/17). M.S. acknowledges the Italian MIUR (2017ZE49E7) and the University of Genoa for funding. M.B. acknowledges financial support from the Deutsche Forschungsgemeinschaft DFG (BE 2413/3-1). Also, this work benefited of EPOS TCS MSL TNA access to Electron Microscopy Facilities, (Utrecht University, The Netherlands), supported by European Community HORIZON 2020 research and innovation program under grant agreement N 676564, and Dutch national funding; Internationalisation in the Earth and Life Sciences – NWO ALWIN.010 – "Implementing the European Plate Observing System (EPOS): Optimizing Dutch leadership of the multi-scale laboratories component". The data presented in this paper are publicly available via the data publication platform of Utrecht University (https://public.yoda.uu.nl/geo/UU01/RVRHHE.html) We are grateful to two anonymous reviewers for their comments.

Appendix A. Supplementary material

Supplementary material related to this article can be found online at https://doi.org/10.1016/j.epsl.2020.116490.

References

Agard, P., Yamato, P., Jolivet, L., Burov, E., 2009. Exhumation of oceanic blueschists and eclogites in subduction zones: timing and mechanisms. Earth-Sci. Rev. 92, 53–79. https://doi.org/10.1016/j.earscirev.2008.11.002.

Andersen, T.B., Austrheim, H., 2006. Fossil earthquakes recorded by pseudotachylytes in mantle peridotite from the Alpine subduction complex of Corsica. Earth Planet. Sci. Lett. 242, 58–72. https://doi.org/10.1016/j.epsl.2005.11.058.

Angiboust, S., Agard, P., Raimbourg, H., Yamato, P., Huet, B., 2011. Subduction interface processes recorded by eclogite-facies shear zones (Monviso, W. Alps). Lithos 127, 222–238. https://doi.org/10.1016/j.lithos.2011.09.004.

Austrheim, H., 2013. Fluid and deformation induced metamorphic processes around Moho beneath continent collision zones: examples from the exposed root zone of the Caledonian mountain belt, W-Norway. Tectonophysics 609, 620–635. https://doi.org/10.1016/j.tecto.2013.08.030.

Beall, A., Fagereng, Å., Ellis, S., 2019. Strength of strained two-phase mixtures: application to rapid creep and stress amplification in subduction zone Mélange. Geophys. Res. Lett. 46, 169–178. https://doi.org/10.1029/2018GL081252.

Barnicoat, A.C., Cartwright, I., 1997. The gabbro–eclogite transformation: an oxygen isotope and petrographic study of west Alpine ophiolites. J. Metamorph. Geol. 15, 93–104. https://doi.org/10.1111/j.1525-1314.1997.00058.x.

Bodinier, J.L., 1988. Geochemistry and petrogenesis of the Lanzo peridotite body, western Alps. Tectonophysics 149, 67–88. https://doi.org/10.1016/0040-1951(88)90119-9.

Brey, G.P., Köhler, T., 1990. Geothermobarometry in four-phase lherzolites II. New thermobarometers, and practical assessment of existing thermobarometers. J. Petrol. 31, 1353–1378. https://doi.org/10.1093/petrology/31.6.1353.

Brudzinski, M.R., Thurber, C.H., Hacker, B.R., Engdahl, E.R., 2007. Global prevalence of double Benioff zones. Science 316, 1472–1474. https://doi.org/10.1093/petrology/31.6.1353.

Debret, B., Nicollet, C., Andreani, M., Schwartz, S., Godard, M., 2013. Three steps of serpentinization in an eclogitized oceanic serpentinization front (Lanzo Massif – Western Alps). J. Metamorph. Geol. 31, 165–186. https://doi.org/10.1111/jmg.12008.

Deschamps, F., Godard, M., Guillot, S., Hattori, K., 2013. Geochemistry of subduction zone serpentinites: a review. Lithos 178, 96–127. https://doi.org/10.1016/j.lithos.2013.05.019.

Di Muro, A., Villemant, B., Montagnac, G., Scaillet, B., Reynard, B., 2006. Quantification of water content and speciation in natural silicic glasses (phonolite, dacite, rhyolite) by confocal microRaman spectrometry. Geochim. Cosmochim. Acta 70, 2868–2884. https://doi.org/10.1016/j.gca.2006.02.016.

Di Muro, A., Métrich, N., Mercier, M., Giordano, D., Massare, D., Montagnac, G., 2009. Micro-Raman determination of iron redox state in dry natural glasses: application to peralkaline rhyolites and basalts. Chem. Geol. 259, 78–88. https://doi.org/10.1016/j.chemgeo.2008.08.013.

Dobson, D.P., Meredith, P.G., Boon, S.A., 2002. Simulation of subduction zone seismicity by dehydration of serpentine. Science 298, 1407–1410. https://doi.org/10.1126/science.1075390.

Fabbri, O., Magott, R., Fournier, M., Etienne, L., 2018. Pseudotachylyte in the Monte Maggiore ophiolitic unit (Alpine Corsica): a possible lateral extension of the Cima di Gratera intermediate-depth Wadati-Benioff paleo-seismic zone. Bull. Soc. Géol. Fr. 189, 18. https://doi.org/10.1051/bsgf/2018020.

Faccenda, M., Gerya, T.V., Burlini, L., 2009. Deep slab hydration induced by bending-related variations in tectonic pressure. Nat. Geosci. 2, 790–793. https://doi.org/10.1038/ngeo656.

Faccenda, M., 2014. Water in the slab: a trilogy. Tectonophysics 614, 1–30. https://doi.org/10.1016/j.tecto.2013.12.020.

Ferrand, T.P., Hilairet, N., Incel, S., Deldicque, D., Labrousse, L., Gasc, J., Renner, J., Wang, Y., Green II, H.W., Schubnel, A., 2017. Dehydration-driven stress transfer triggers intermediatedepth earthquakes. Nat. Commun. 8, 15247. https://doi.org/10.1038/ncomms15247.

Gilio, M., Scambelluri, M., Agostini, S., Godard, M., Peters, D., Pettke, T., 2019. Petrology and geochemistry of serpentinites associated with the ultra-high pressure Lago di Cignana Unit (Italian Western Alps). J. Petrol. 60, 1229–1262. https://doi.org/10.1093/petrology/egz030.

Grevemeyer, I., Hayman, N.W., Lange, D., Peirce, C., Papenberg, C., Van Avendonk, H.J.A., Schmid, F., Gómez de La Peña, L., Dannowski, A., 2019. Constraining the maximum depth of brittle deformation at slow- and ultraslow-spreading ridges using microseismicity. Geology 47, 1069–1073. https://doi.org/10.1130/G46577.1.

Hacker, B.R., Peacock, S.M., Abers, G.A., Holloway, S.D., 2003. Subduction factory 2. Are intermediate-depth earthquakes in subducting slabs linked to metamorphic dehydration reactions? J. Geophys. Res. 108 (B1), 2030. https://doi.org/10.1029/2001JB001129.

Hawemann, F., Mancktelow, N., Wex, S., Camacho, A., Pennacchioni, G., 2018. Pseudotachylyte as field evidence for lower crustal earthquakes during the intracontinental Petermann Orogeny (Musgrave Block, Central Australia). Solid Earth 9, 629–648. https://doi.org/10.5194/se-9-629-2018.

Incel, S., Schubnel, A., Renner, J., John, T., Labrousse, L., Hilairet, N., Freeman, H., Wang, Y., Renard, F., Jamtveit, B., 2019. Experimental evidence for wall-rock pulverization during dynamic rupture at ultra-high pressure conditions. Earth Planet. Sci. Lett. 528, 115832. https://doi.org/10.1016/j.epsl.2019.115832.

Jamtveit, B., Ben-Zion, Y., Renard, F., Austheim, H., 2018. Earthquake-induced transformation of the lower crust. Nature 556, 487–491. https://doi.org/10.1038/s41586-018-0045-y.

Jamtveit, B., Petley-Ragan, A., Incel, S., Dunkel, K.G., Aupart, C., Austrheim, H., et al., 2019. The effects of earthquakes and fluids on the metamorphism of the lower continental crust. J. Geophys. Res., Solid Earth 124, 7725–7755. https://doi.org/10.1029/2018JB016461.

John, T., Medvedev, S., Rüpke, L.H., Andersen, T.B., Podladchikov, Y.Y., Austrheim, H., 2009. Generation of intermediate-depth earthquakes by self-localizing thermal runaway. Nat. Geosci. 2, 137–140. https://doi.org/10.1038/ngeo419.

Jung, H., Green II, H., Dobrzhinetskaya, L., 2004. Intermediate-depth earthquake faulting by dehydration embrittlement with negative volume change. Nature 428, 545–549. https://doi.org/10.1038/nature02412.

Kaczmarek, M.-A., Müntener, O., 2008. Juxtaposition of melt impregnation and high temperature shear zone in the upper mantle; field and petrological constraints from the Lanzo peridotite (Northern Italy). J. Petrol. 49, 2187–2220. https://doi.org/10.1093/petrology/egn065.

Kawakatsu, H., 1985. Double seismic zone in Tonga. Nature 316, 53–55.

Kelemen, P.B., Hirth, G.A., 2007. Periodic shear-heating mechanism for intermediate-depth earthquakes in the mantle. Nature 446, 787–790. https://doi.org/10.1038/nature05717.

Kienast, J.R., Pognante, U., 1988. Chloritoid bearing assemblages in eclogitized metagabbros of the Lanzo peridotite body (Western Italian Alps). Lithos 21, 1–11. https://doi.org/10.1016/0024-4937(88)90002-3.

Kirby, S., Engdahl, E.R., Denlinger, R., 1996. Intermediate-depth earthquakes and arc volcanism as physical expressions of crustal and upper mantle metamorphism. In: Bebout, G.E., Scholl, D.W., Kirby, S.H., Platt, J.P. (Eds.), Subduction Top to Bottom. American Geophysical Union, pp. 195–214.

Kita, S., Okada, T., Nakajima, J., Matsuzawa, T., Hasegawa, A., 2006. Existence of a seismic belt in the upper plane of the double seismic zone extending in the along-arc direction at depths of 70–100 km beneath NE Japan. Geophys. Res. Lett. 33, L24310. https://doi.org/10.1029/2006GL028239.

Korenaga, J., 2017. On the extent of mantle hydration caused by plate bending. Earth Planet. Sci. Lett. 457, 1–9. https://doi.org/10.1016/j.epsl.2016.10.011.

Locatelli, M., Verleguet, A., Agard, P., Federico, L., Angiboust, S., 2018. Intermediate-depth brecciation along the subduction plate interface (Monviso eclogite, W. Alps). Lithos 320–321, 378–402. https://doi.org/10.1016/j.lithos.2018.09.028.

Menegon, L., Pennacchioni, G., Malaspina, N., Harris, K., Wood, E., 2017. Earthquakes as precursors of ductile shear zones in the dry and strong lower crust. Geochem. Geophys. Geosyst. 18, 4356–4374. https://doi.org/10.1002/2017GC007189.

Nimis, P., Grütter, H., 2010. Internally consistent geothermometers for garnet peridotites and pyroxenites. Contrib. Mineral. Petrol. 159, 411–427. https://doi.org/10.1007/s00410-009-0455-9.

Nimis, P., Taylor, W.R., 2000. Single-clinopyroxene thermobarometry for garnet peridotites. Part I. Calibration and testing of a Cr-in-Cpx barometer and an enstatite-in-Cpx thermometer. Contrib. Mineral. Petrol. 139, 541–554. https://doi.org/10.1007/s004100000156.

Peacock, S.M., 2001. Are the lower planes of double seismic zones caused by serpentine dehydration in subducting oceanic mantle? Geology 29, 299–302. https://doi.org/10.1130/0091-7613(2001)029<0299:ATLPOD>2.0.CO;2.

Pelletier, L., Müntener, O., 2006. High-pressure metamorphism of the Lanzo peridotite and its oceanic cover, and some consequences for the Sesia-Lanzo zone (northwestern Italian Alps). Lithos 90, 111–130. https://doi.org/10.1016/j.lithos.2006.01.006.

Petley-Ragan, A., Ben-Zion, Y., Austrheim, H., Ildefonse, B., Renard, F., Jamtveit, B., 2019. Dynamic earthquake rupture in the lower crust. Sci. Adv. 5, eaaw0913. https://doi.org/10.1126/sciadv.aaw0913.

Piccardo, G.B., Ranalli, G., Marasco, M., Padovano, M., 2007. Ultramafic pseudotachylytes in the Mt. Moncuni peridotite (Lanzo Massif, Western Alps): tectonic evolution and upper mantle seismicity. Period. Mineral. 76, 181–197. https://doi.org/10.2451/2007PM0024.

Piccardo, G.B., Ranalli, G., Guarnieri, L., 2010. Seismogenic shear zones in the lithospheric mantle: ultramafic pseudotachylytes in the Lanzo peridotite (Western Alps, NW Italy). J. Petrol. 51, 81–100. https://doi.org/10.1093/petrology/egp067.

Plümper, O., John, T., Podladchikov, Y.Y., Vrijmoed, J.C., Scambelluri, M., 2017. Fluid escape from subduction zones controlled by channel-forming reactive porosity. Nat. Geosci. 10, 150–156. https://doi.org/10.1038/NGEO2865.

Scambelluri, M., Cannaò, E., Gilio, M., 2019. The water and fluid-mobile element cycles during serpentinite subduction. A review. Eur. J. Mineral. 31, 405–428. https://doi.org/10.1127/ejm/2019/0031-2842.

Scambelluri, M., Pennacchioni, G., Gilio, M., Bestmann, M., Plümper, O., Nestola, F., 2017. Fossil intermediate-depth earthquakes in subducting slabs linked to differential stress release. Nat. Geosci. 10, 960–966. https://doi.org/10.1038/s41561-017-0010-7.

Seno, T., Yamanaka, Y., 1996. Double seismic zones, compressional deep trench–outer rise events, and superplumes. In: Bebout, G.E., et al. (Eds.), Subduction Top to Bottom. In: Geophys. Monogr. Ser., vol. 96. AGU, Washington, D.C., pp. 347–355.

Sibson, R.H., 1975. Generation of pseudotachylyte by ancient seismic faulting. Geophys. J. R. Astron. Soc. 43, 775–794.

Stein, C.A., Stein, S., 1994. Constraints on hydrothermal heat flux through the oceanic lithosphere from global heat flow. J. Geophys. Res. 99, 3081–3095. https://doi.org/10.1029/93JB02222.

Ranero, C.R., Morgan, J.P., McIntosh, K., Reichert, C., 2003. Bendingrelated faulting and mantle serpentinization at the Middle America trench. Nature 42, 367–373. https://doi.org/10.1038/nature01961.

Reynard, B., Nakajima, J., Kawakatsu, H., 2010. Earthquakes and plastic deformation of anhydrous slab mantle in double Wadati-Benioff zones. Geophys. Res. Lett. 37, L24309. https://doi.org/10.1029/2010GL045494.

Umino, N., Hasegawa, A., 1975. On the two-layered structure of deep seismic plane in northeastern Japan arc. J. Seismol. Soc. Jpn. 27, 125–139.

Yamasaki, T., Seno, T., 2003. Double seismic zone and dehydration embrittlement of the subducting slab. J. Geophys. Res. 108 (B4), 2212. https://doi.org/10.1029/2002JB001918.